*Journal of Engineering Mathematics* **36:** 327–348, 1999.


# Preventing buoyancy-driven flows of two Bingham fluids in a closed pipe – Fluid rheology design for oilfield plug cementing

I. A. FRIGAARD[1*] and J. P. CRAWSHAW[2]
[1]*Schlumberger Dowell, 26 rue de la Cavée, 92140 Clamart, France. e-mail: frigaard@clamart.srpc.slb.com*
[2]*Schlumberger Cambridge Research, High Cross, Madingley Road, Cambridge, CB3 0EL, England*
*e-mail: crawshaw@cambridge.scr.slb.com*

Received 21 July 1998; accepted in revised form 3 February 1999

**Abstract.** The mechanically unstable situation of a heavy Bingham fluid resting on top of a light Bingham fluid in an inclined closed-ended pipe can be stabilised if the fluids have sufficiently large yield stresses. This paper focuses on determining the yield stresses that are sufficient to keep the fluids statically stable for a given fluid density difference, pipe diameter and pipe inclination. The results are applicable to a broad class of practically observable flows. This situation provides an idealised model for the oilfield process of plug cementing.

**Key words:** Bingham fluids, multi-layer flow, no-flow/yield criteria, stability, variational methods.

## 1. Introduction

Many industrial fluids are characterised by a rheology that exhibits a yield stress [1], and one of the simplest constitutive models is that of a Bingham fluid or plastic. When such a fluid fills a pipe and is subjected to an axial pressure gradient, it flows only if a given critical pressure gradient is exceeded. Thus, Bingham fluids are able to support nonzero deviatoric stresses whilst at rest. The critical pressure gradient (or alternatively critical yield stress or critical pipe diameter), may be found either by straightforward physical arguments [2], or by rigorous analytic methods [3, pp. 78–82], [4].

Consider two Bingham fluids of differing densities ($\hat{\rho}_k$) and rheologies ($\hat{\mu}_k$, $\hat{\tau}_{k,Y}$), which are miscible, but do not mix significantly. Suppose that an inclined closed-ended pipe is filled with both fluids, separated by a clean interface and with the heavier fluid on top of the lighter fluid (see Figure 1). This situation is mechanically unstable. Without a yield stress in either fluid (*e.g.* two Newtonian fluids), the fluids will flow in such a way as to eventually exchange positions. The underlying cause of the unstable motion is a buoyancy force, arising from the density difference between the fluids.

The initial condition for this type of flow includes the specification of the interface position. For two Newtonian fluids, it becomes immediately clear that there will be only one interface configuration for which the fluids may remain static (namely an interface which lies perpendicular to the direction of gravity), but that this interface is unconditionally unstable. For two Bingham fluids, the static stability problem is quite different. Firstly, by analogy with the Bingham fluid pipe flow described above, it is expected that for sufficiently large yield stresses, $\hat{\tau}_{k,Y}$, the buoyancy driven flow will be stopped. Indeed, for an infinitely long pipe,

* Corresponding author.

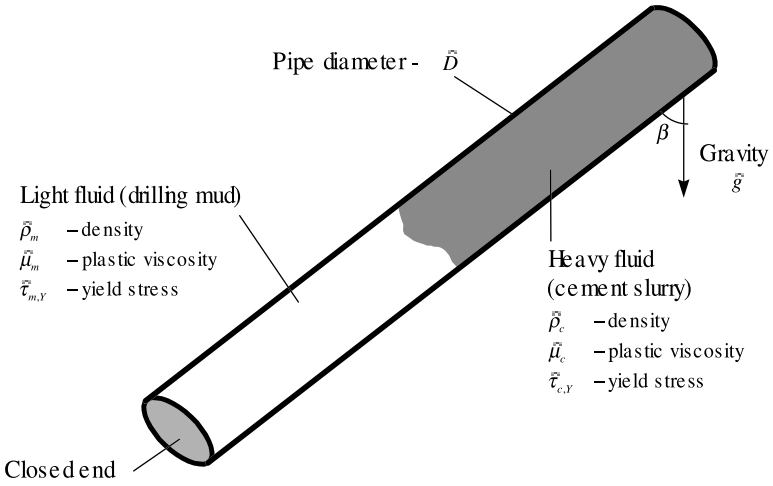


*Figure 1.* An idealised fluid flow model for plug-cementing.

a simple dimensionless analysis suggests that the existence of this static situation will be governed by the angle of inclination $\beta$, and the following two dimensionless groups

$$\tau_{c,Y} = \frac{\hat{\tau}_{c,Y}}{[\hat{\rho}_c - \hat{\rho}_m]\hat{g}\hat{D}}, \qquad \tau_{m,Y} = \frac{\hat{\tau}_{m,Y}}{[\hat{\rho}_c - \hat{\rho}_m]\hat{g}\hat{D}}. \tag{1}$$

In (1), the two fluids are distinguished by the subscripts $c$ and $m$ ($c$ denoting the heavier fluid), $\hat{g}$ is the gravitational acceleration and $\hat{D}$ is the pipe diameter; (dimensional quantities are denoted by a *hat* symbol, $\hat{\cdot}$, and dimensionless variables without). A second major difference in the Bingham fluid problem is that infinitely many static interface configurations should be possible, *e.g.* small perturbations from the unique Newtonian static solution should generate correspondingly small deviatoric stresses at the interface, which small finite yield stresses are able to resist. Finally, it is expected that the static solutions will be either conditionally or absolutely stable, again depending on the size of the yield stresses.

The industrial interest in such flows stems from the oilfield operation of plug-cementing. In this process, one attempts to place a heavy cement slurry above a lighter drilling mud. Alternatively, a *viscous pill* fluid of intermediate density is placed between the mud and cement. A typical lengthscale for an oil well is $\sim 10^3$ m and diameter $\sim 0{\cdot}3$ m; lengths of the fluid stages involved are typically $\geqslant 30$ m. The aim is to maintain the cement slurry statically positioned in the well for a period of many hours while it sets. Cement plugs can be used either to hydraulically seal the well (*i.e. abandonment* plug or *lost-circulation* plug), or as a mechanical aid to changing the direction of the well trajectory during drilling (*kick-off* plug). This process and a range of technical issues are discussed in [5–8], [9, Chapter 13], [10]. Often there are density constraints on the fluids that are used for plug cementing. However, rheological parameters may be varied by chemical means to attain given stability design limits. This paper attempts to define those limits.

For fixed inclination and interface, it must be expected that the two dimensionless yield stresses ($\tau_{k,Y}, k = c, m$), interact in determining the limit of static stability. In general the limit is unknown and this paper considers how to estimate the limit for a class of physically realistic fluid-fluid interfaces.

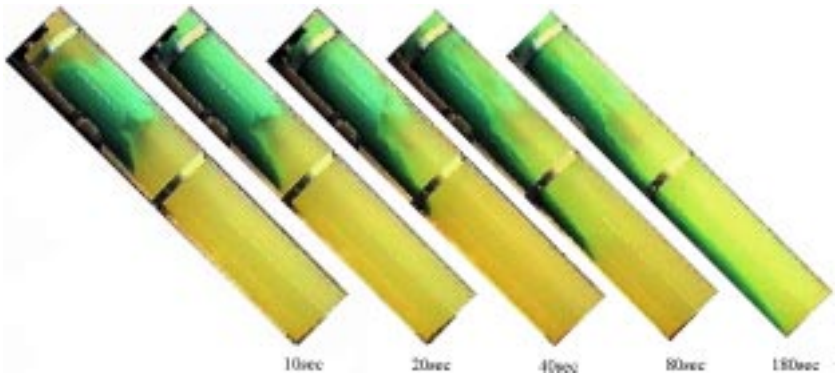

*Figure 2.* A slumping exchange flow observed in an experimental rig at Schlumberger Cambridge Research (UK) at different times after placement; density difference 1: 1·1 SG, $D = 0{\cdot}2\,\mathrm{m}$, $\beta = 45$ degrees.

Much of the paper develops qualitative results using variational methods. These methods are favoured here since the interface is not determined *a priori* in the industrial application. Additionally, the problem of determining limiting stability states has more in common with studies of plasticity (where such methods are more common), than with classical fluid mechanics. A further question is whether or not direct computation could have sensibly replaced either the approximate results derived or the validation experiments performed. Displacement and filling flows are modelled within many modern computational fluid mechanics software tools and the geometry here is relatively simple. The drawback in using computational methods is in the way in which the Bingham fluid rheology is approximated for computation. For very low rates of strain the plastic yielding behaviour is typically replaced by that of a very viscous Newtonian fluid. This is a numerically motivated perturbation of the constitutive laws. It has the consequence that mechanically unstable flows never cease to flow. Exactly how numerical results are to be rigorously interpreted, how a zero-flow limit is to be determined and indeed whether or not the (rheological) perturbation is itself regular in this limit are difficult questions.

An experimental observation, when the fluid properties are such that the flow is somehow *close* to the limit of not flowing, is that the heavy fluid slides down the lower side of the pipe, displacing the lighter fluid up the higher side of the pipe. Figure 2 shows a series of still pictures taken from a video of this motion, observed in an experimental rig at Schlumberger Cambridge Research (UK). Such motions are also reported in [7]. This is a slumping motion in which the bulk of the two fluids moves axially at a slow pace. The velocity field may therefore be thought of as being near-uniaxial, except close to the two displacement fronts where a three-dimensional flow must exist in some sort of transition region (see schematic in Figure 3). It is also noted that although the eventual flow is observed to propagate uniaxially, the initiation can often involve a multi-dimensional flow.

The propagating flows described above are slow stratified axial flows, generally starting with low kinetic energies. The main aim of this paper is to derive sufficient conditions on $\tau_{k,Y}$, $k = c, m$, such that flows which may start from fairly arbitrary initial conditions, will not propagate axially. In the central region of Figure 3 the flow is characterised by near-uniaxial streamlines and by there being no net volumetric flux in the direction of the pipe axis, (*i.e.* the flow of the cement down the incline is matched by the *exchange* flow of the mud up the incline). Such flows have been studied both in slots [11] and in pipes/general ducts [12–13].

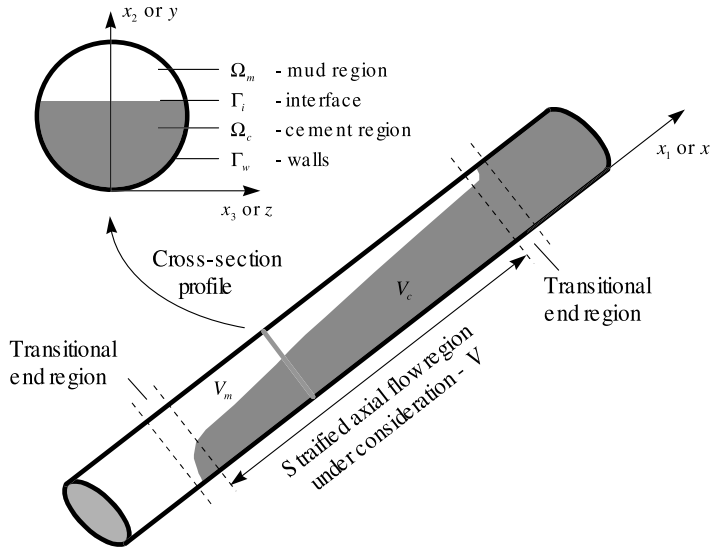


*Figure 3.* Schematic of stratified axial flow region considered, pipe geometry, coordinates and pipe cross-sectional notation.

The important difference between this work and [11–13] is that normal deviatoric stresses, which are generated at the end regions of the flow, are completely ignored in [11–13], but are included here. This makes experimental comparison possible, see Section 6.

A brief outline of the paper is as follows. Section 2 derives the dimensionless model equations and deals with the issue of model closure. Section 3 investigates various qualitative properties of the axial velocity solution. Stress minimisation principles are considered in Section 4. Section 5 combines estimates of the normal deviatoric stresses with the results of [13]. In doing so, a surface is derived in the three-dimensional $(\beta, \tau_{c,Y}, \tau_{m,Y})$-space which defines conditions for the axial velocity to be zero. Experimental comparison is made in Section 6. The paper concludes with a discussion of the practical application and limitations of this work, in Section 7.

## 2. Dimensionless model equations

Consider the type of slow, stratified slumping flow described in Section 1. Away from the end regions of the flow, both fluid streamlines and fluid-fluid interfaces are assumed to be near-parallel to the pipe axis. This intermediate flowing region is denoted $V(\hat{t}\,)$, and is divided into two distinct fluid regions: $V_c(\hat{t}\,)$ and $V_m(\hat{t}\,)$ (cement and mud). The incompressible Navier–Stokes equations are valid in each fluid region with no-slip conditions on the pipe walls. Capillarity and molecular difusion effects are assumed insignificant on the time and length-scales considered. The interfaces are then simply advected with the flow. Velocity and stress (traction) vectors are continuous across all fluid-fluid interfaces. The assumption is made that the interfaces evolve in such a way that they always remain near parallel to the pipe axis, within the volume $V(\hat{t}\,)$, *e.g.* $V(\hat{t}\,)$ might expand axially along the pipe in both directions, *stretching* the interface in the middle, *new* interface being created in the end transition regions.

Coordinates $\hat{\mathbf{x}}$ are as defined in Figure 3 and are scaled differentially in axial and nonaxial directions. Let $\hat{L}$ be an axial length-scale and $\hat{D}$ the pipe diameter. Spatial coordinates and derivatives are scaled as follows

$$x_1 = \frac{\hat{x}_1}{\hat{L}}, \qquad x_2 = \frac{\hat{x}_2}{\hat{D}}, \qquad x_3 = \frac{\hat{x}_3}{\hat{D}}. \tag{2}$$

The ratio between $\hat{L}$ and $\hat{D}$ is denoted[1] $\delta$

$$\delta = \frac{\hat{D}}{\hat{L}} \ll 1, \tag{3}$$

The pressure and velocity are denoted $\hat{p}(\hat{\mathbf{x}}, \hat{t}\,)$ and $\hat{\mathbf{u}}(\hat{\mathbf{x}}, \hat{t}\,)$. The stress and deviatoric stress tensors are denoted $\hat{\sigma}_{k,ij}$ and $\hat{\tau}_{k,ij}$, for $k = c, m$. Let $\hat{u}_*$ denote a typical axial velocity of the flow, which is used to scale the velocity as follows

$$\hat{\mathbf{u}} = \hat{u}_*(u_1, \delta u_2, \delta u_3) \tag{4}$$

and to define the timescale $\hat{t}_* \equiv \hat{L}/\hat{u}_*$.

The (positive) density difference $\Delta\hat{\rho}$ is defined by $\Delta\hat{\rho} = \hat{\rho}_c - \hat{\rho}_m$ and is used to define

$$\phi_c \equiv \frac{\hat{\rho}_c}{\Delta\hat{\rho}}, \qquad \phi_m \equiv \frac{\hat{\rho}_m}{\Delta\hat{\rho}} = \phi_c - 1. \tag{5}$$

A dimensionless modified pressure is defined by

$$p(\mathbf{x}, t) = \frac{\hat{p}(\hat{\mathbf{x}}, \hat{t}\,) - \hat{p}_0 + \hat{\rho}_m\hat{g}[\hat{x}_1 \cos\beta + \hat{x}_2 \sin\beta]}{\Delta\hat{\rho}\hat{g}\hat{L}}, \tag{6}$$

where $\hat{p}_0$ denotes a reference pressure at the origin.

For the flow to be noninertial there should exist a balance between the leading-order deviatoric stress gradients and the buoyancy gradient

$$\frac{\hat{\tau}_{k,ij}}{\hat{D}} \sim \Delta\hat{\rho}\hat{g}. \tag{7}$$

In yielded regions of the flow, the velocity and length-scales adopted imply that $\hat{\tau}_{k,12}$ and $\hat{\tau}_{k,13}$ are dominant. In unyielded flow regions, the stress is indeterminate, and the deviatoric stress components need not be scaled according to the prescribed velocity and length-scales. Consider for example, a horizontal pipe with the two fluids separated by a vertical interface. Across this interface the density difference implies a static pressure difference, which must be balanced by a difference in $\hat{\tau}_{k,11}$. More generally, any interface in the transitional end regions that is perpendicular to the pipe axis can generate a static pressure differential that, in the limit of a static flow, implies $\hat{\tau}_{k,11} \sim \Delta\hat{\rho}\hat{g}\hat{D}$. Since also

$$\hat{\tau}_{k,11} + \hat{\tau}_{k,22} + \hat{\tau}_{k,33} = 0, \tag{8}$$

[1] Often $\delta \ll 1$ is an overly restrictive assumption on $\hat{L}$ for *long-thin* flows of Bingham fluids. Yielded flow regions typically have a layer width much smaller than the pipe diameter $\hat{D}$. A much shorter axial length-scale is therefore needed for the flow to be considered as near-uniaxial.

by definition of the deviatoric stress tensor, the scaling assumed[2] is as follows

$$\tau_{k,ij} \equiv \frac{\hat{\tau}_{k,ij}}{\Delta\hat{\rho}\hat{g}\hat{D}}, \quad i,j \neq 2,3; \qquad \tau_{k,23} \equiv \frac{\hat{\tau}_{k,23}}{\Delta\hat{\rho}\hat{g}\hat{L}}, \tag{9}$$

### 2.1. LEADING-ORDER MODEL

Following the above scaling, the dimensionless field equations for $\mathbf{x} \in V_k$ are

$$\frac{\phi_k\hat{u}_*^2}{\hat{g}\hat{L}}\frac{\mathrm{d}u_1}{\mathrm{d}t} = -\frac{\partial p}{\partial x_1} - (\phi_k - \phi_m)\cos\beta + \frac{\partial\tau_{k,12}}{\partial x_2} + \frac{\partial\tau_{k,13}}{\partial x_3} + \delta\frac{\partial\tau_{k,11}}{\partial x_1}, \tag{10}$$

$$\delta^2\frac{\phi_k\hat{u}_*^2}{\hat{g}\hat{L}}\frac{\mathrm{d}u_2}{\mathrm{d}t} = -\frac{\partial p}{\partial x_2} - (\phi_k - \phi_m)\delta\sin\beta + \delta\frac{\partial\tau_{k,22}}{\partial x_2} + \delta^2\left[\frac{\partial\tau_{k,12}}{\partial x_1} + \frac{\partial\tau_{k,23}}{\partial x_3}\right], \tag{11}$$

$$\delta^2\frac{\phi_k\hat{u}_*^2}{\hat{g}\hat{L}}\frac{\mathrm{d}u_3}{\mathrm{d}t} = -\frac{\partial p}{\partial x_3} + \delta\frac{\partial\tau_{k,33}}{\partial x_3} + \delta^2\left[\frac{\partial\tau_{k,13}}{\partial x_1} + \frac{\partial\tau_{k,23}}{\partial x_2}\right], \tag{12}$$

$$\frac{\partial u_j}{\partial x_j} = 0. \tag{13}$$

Neglecting terms of $O(\delta)$ and making the following noninertial assumption

$$\frac{\phi_k\hat{u}_*^2}{\hat{g}\hat{L}} \ll 1, \tag{14}$$

the leading-order momentum equations are

$$\cos\beta - f = \frac{\partial\tau_{c,12}}{\partial x_2} + \frac{\partial\tau_{c,13}}{\partial x_3}, \quad \mathbf{x} \in \Omega_c, \tag{15}$$

$$-f = \frac{\partial\tau_{m,12}}{\partial x_2} + \frac{\partial\tau_{m,13}}{\partial x_3}, \quad \mathbf{x} \in \Omega_m, \tag{16}$$

$$f = f(x_1), \tag{17}$$

where $\Omega_c$ and $\Omega_m$ denote the cross-sectional areas of the pipe that are occupied by cement and mud respectively. The parameter $-f$ that appears above is the dimensionless modified pressure gradient

$$f \equiv -\frac{\partial p}{\partial x_1}. \tag{18}$$

[2] For the model only $\tau_{k,23}$ is assumed to be small with respect to the other deviatoric stress components. This is the consequence of the velocity and length-scaling. Without any such assumption on $\tau_{k,23}$ the flow must be considered fully three-dimensional, whereas the aim here is to take advantage of the near uniaxial nature of the flow.

Recall that the hydrostatic mud pressure has been subtracted from the pressure before scaling. The modified pressure gradient in the cement is $\cos\beta - f$. Typically, its expected that $f \in [0, \cos\beta]$ so that the mud is pushed up the incline and the cement down the incline.

The interception of the interface with the cross-section is denoted $\Gamma_i$, with normal in the pipe cross-section, $\mathbf{n} = (\delta n_1, n_2, n_3)$. Leading-order stress continuity conditions on $\Gamma_i$ are

$$p_m + n_2^2\tau_{m,22} + n_3^2\tau_{m,33} = p_c + n_2^2\tau_{c,22} + n_3^2\tau_{c,33}, \tag{19}$$

$$\tau_{c,22} - \tau_{c,33} = \tau_{m,22} - \tau_{m,33}, \tag{20}$$

$$n_2\tau_{c,12} + n_3\tau_{c,13} = n_2\tau_{m,12} + n_3\tau_{m,13}. \tag{21}$$

These conditions come simply from continuity of $\mathbf{n}\cdot\boldsymbol{\sigma}_k$ across the interface. The velocity is continuous across $\Gamma_i$ and on the walls the velocity satisfies

$$\mathbf{u} = 0. \tag{22}$$

2.1.1. *Constitutive equations and closure*

The dimensionless plastic viscosities $\mu_k$, are defined in terms of the dimensional model parameters by

$$\mu_k = \frac{\hat{\mu}_k\hat{u}_*}{\Delta\hat{\rho}\hat{g}\hat{D}^2}, \quad k = c, m. \tag{23}$$

Equations (15) and (16) are similar to the leading-order model derived and analysed in [12–13]. This leading-order model is an axial flow model, in which the velocity component $u_1$ is to be determined. The aim of the analysis here is not to find solutions to the axial flow problem, but instead to find practical conditions under which only the trivial solution $u_1 = 0$ exists. The leading-order momentum equations also do not determine the deviatoric stress components $\tau_{k,ii}$. By assumption, spatial variations in each $\tau_{k,ii}$ in the direction $x_1$ are $O(\delta)$ smaller than those in the nonaxial directions $x_2$ and $x_3$. A general leading-order form for the terms $\tau_{k,ii}$, in any cross-section within $V$, is therefore: $\tau_{k,ii} = \tau_{k,ii}(x_2, x_3) + O(\delta)$, $i = 1, 2, 3$. Define $\tau_{k,n}(x_2, x_3)$ on each pipe cross-section by

$$\tau_{k,n}(x_2, x_3) \equiv \tfrac{1}{2}[\tau_{k,11}^2 + \tau_{k,22}^2 + \tau_{k,33}^2]^{1/2}. \tag{24}$$

The function $\tau_{k,n}(x_2, x_3)$ is regarded as data for the problem. It is supposed that $\tau_{k,n}(x_2, x_3)$ is continuous within $\Omega_k$ and that (19) and (20) are satisfied. Additionally, only those $\tau_{k,n}(x_2, x_3)$ are considered

$$\tau_{k,n}(x_2, x_3) \leqslant \tau_{k,Y} - \xi, \tag{25}$$

for some $\xi > 0$, *i.e.* it is assumed that the stresses $\tau_{k,n}$ generated at the ends of $V$ are insufficient alone to allow the fluids to yield and flow in $V$.

To understand the effect of imposing a stress distribution $\tau_{k,n}(x_2, x_3)$ on the flow, consider the (dimensionless) rate of strain of the three-dimensional problem, within $\Omega$, *i.e.* $\dot{\gamma}(\mathbf{u})$.

Firstly, consider where $\dot{\gamma}(\mathbf{u}) \gg \delta$. In this region the gradients of the axial velocity component dominate and

$$\dot{\gamma}(\mathbf{u}) \sim \dot{\gamma}(u_1) \equiv \left[ \left( \frac{\partial u_1}{\partial x_2} \right)^2 + \left( \frac{\partial u_1}{\partial x_3} \right)^2 \right]^{1/2}. \tag{26}$$

The leading-order deviatoric stresses are

$$\tau_{k,1j} = \left[ \mu_k + \frac{\tau_{k,Y}}{\dot{\gamma}(u_1)} \right] \frac{\partial u_1}{\partial x_j}, \quad k = c, m, \quad j = 2, 3. \tag{27}$$

Secondly, consider where $\dot{\gamma}(\mathbf{u}) \sim \delta$, but $\dot{\gamma}(\mathbf{u}) \neq 0$. Here

$$\tau_{k,1j} = \left[ \mu_k + \frac{\tilde{\tau}_{k,Y}(x_2, x_3)}{\dot{\gamma}(u_1)} \right] \frac{\partial u_1}{\partial x_j}, \quad k = c, m, \quad j = 2, 3, \tag{28}$$

where

$$\tilde{\tau}_{k,Y}(x_2, x_3) \equiv \tau_{k,Y} \frac{\dot{\gamma}(u_1(x_2, x_3))}{\dot{\gamma}(\mathbf{u}(x_2, x_3))}. \tag{29}$$

It is noted from (25) that in this region, $\dot{\gamma}(u_1) \neq 0$ and

$$\xi + O(\delta) < \tilde{\tau}_{k,Y}(x_2, x_3) \leqslant \tau_{k,Y}. \tag{30}$$

Finally, consider the region where $\dot{\gamma}(\mathbf{u}) = 0$, implying also that $\dot{\gamma}(u_1) = 0$. In this region the deviatoric stresses are indeterminate.

Combining the above analysis, leading-order constitutive equations can be defined everywhere by

$$\dot{\gamma}(u_1) > 0 \Rightarrow \begin{cases} \tau_{k,12} = \left[ \mu_k + \dfrac{\tau_{k,R}(x_2, x_3)}{\dot{\gamma}(u_1)} \right] \dfrac{\partial u_1}{\partial x_2}, & k = c, m, \\ \tau_{k,13} = \left[ \mu_k + \dfrac{\tau_{k,R}(x_2, x_3)}{\dot{\gamma}(u_1)} \right] \dfrac{\partial u_1}{\partial x_3}, & k = c, m, \end{cases} \tag{31}$$

and

$$\dot{\gamma}(u_1) = 0 \Leftrightarrow \tau_k \leqslant \tau_{k,R}(x_2, x_3), \quad k = c, m, \tag{32}$$

where the *reduced* yield stress $\tau_{k,R}(x_2, x_3)$ will be defined by either $\tau_{k,Y}$ or $\tilde{\tau}_{k,Y}(x_2, x_3)$, depending on $\dot{\gamma}(\mathbf{u})$.

Formally, defining $\tau_{k,R}(x_2, x_3)$ depends on the solution to the three-dimensional problem, which in general can not be constructed from the axial velocity component (but see [14] for an asymptotic analysis of flow in a narrow eccentric annulus). Thus, for simplicity only the closure $\tau_{k,R} = \tau_{k,R}(x_2, x_3)$ is considered, *i.e.* a form of linearisation (although the problem still remains nonlinear). The important thing to note is that the effect of the imposed stresses $\tau_{k,n}(x_2, x_3)$ is to effectively *reduce* the yield stresses to $\tau_{k,R}(x_2, x_3)$, where $\tau_{k,R}(x_2, x_3) > 0$, due to (25), and $\tau_{k,R}(x_2, x_3)$ can be expected to be continuous in each $\Omega_k$.

2.1.2. *Problem summary*

To summarise the result of the foregoing derivation, the problem has been reduced to a set of leading-order equations for the axial component of velocity, $u_1$. The classical formulation of this problem consists of Equations (15) and (16), the constitutive relations (32) and (31), boundary condition at the wall

$$u_1 = 0, \tag{33}$$

and the following continuity conditions on each fluid-fluid interface

$$u_1 = u_{\text{int}}, \tag{34}$$

$$n_2\tau_{c,12} + n_3\tau_{c,13} = n_2\tau_{m,12} + n_3\tau_{m,13}, \tag{35}$$

(*i.e.* $u_1 = u_{\text{int}}$ from both sides of the interface). The data prescribed for this problem consists of the two fluid domains $\Omega_c$ and $\Omega_m$, the two fluid viscosities, $\mu_k > 0$, $k = c, m$, the two yield stresses $\tau_{k,Y} > 0$, and the two reduced yield stress functions $\tau_{k,R}$, $k = c, m$, which are strictly positive, continuous and bounded (by $\tau_{k,Y}$), in each domain.

## 2.2. VARIATIONAL FORMULATION

Due to the uncertain forms of $\tau_{k,R}$ and $\Omega_k$, $k = c, m$, general results for the classical formulation are hard to derive. Instead a variational formulation is considered. For simplicity of notation, the subscript on $u_1$ is dropped and the coordinates are redefined $(x, y, z) = (x_1, x_2, x_3)$. For arbitrary $u, v \in H_0^1(\Omega)$ define the following norms and functionals

$$a_k(u, v) = \int_{\Omega_k} \frac{\partial u}{\partial y}\frac{\partial v}{\partial y} + \frac{\partial u}{\partial z}\frac{\partial v}{\partial z}\,\mathrm{d}\Omega, \quad k = c, m,$$

$$j_k(v) = \int_{\Omega_k} \tau_{k,R}\left[\left(\frac{\partial v}{\partial y}\right)^2 + \left(\frac{\partial v}{\partial z}\right)^2\right]^{1/2}\mathrm{d}\Omega, \quad k = c, m,$$

$$a_0(u, v) = a_c(u, v) + a_m(u, v),$$

$$a(u, v) = \mu_c a_c(u, v) + \mu_m a_m(u, v),$$

$$j(v) = j_c(v) + j_m(v),$$

$$Q_k(v) = \int_{\Omega_k} v\,\mathrm{d}\Omega, \quad k = c, m,$$

$$Q(v) = Q_c(v) + Q_m(v),$$

$$\|v\|_{L^1(\Omega)} = \int_\Omega |v|\,\mathrm{d}\Omega,$$

$$\|v\|^2_{L^2(\Omega)} = \int_\Omega v^2\,\mathrm{d}\Omega,$$

$$\|v\|^2_{H^1(\Omega)} = \|v\|^2_{L^2(\Omega)} + a_0(v, v),$$

$$L(v) = f\,Q(v) - \cos\beta\, Q_c(v) = -(\cos\beta - f)\,Q(v) + \cos\beta\, Q_m(v).$$

The variational problem for the axial velocity $u$ is to find $u \in H^1_0(\Omega)$ satisfying

$$a(u, v-u) + j(v) - j(u) \geqslant L(v-u), \quad \forall v \in H^1_0(\Omega), \quad u \in H^1_0(\Omega). \tag{36}$$

The derivation of (36) from the classical problem proceeds almost exactly as in [12] and this is not restated. Two different problems may be considered

(1) *General flow*: In this problem, $f$ is a specified constant and the solution only involves determining $u$ satisfying (36).
(2) *Exchange flow*: In this problem, $f \in [F_1, F_2]$ is a constant parameter, which must be determined with $u$ as part of the solution, in such a way that both (36) and

$$Q(u) = 0, \tag{37}$$

are satisfied.

Physically, for the exchange flow problem there will be zero net volumetric flux in the axial direction. The question then is which axial pressure gradient $f$ allows this to happen. Solutions to the general flow problem that do not satisfy (37) correspond to flows for which a nonzero volumetric flow rate is pumped along the pipe. These flows also have practical relevance, but for the problem at hand the ends of the pipe (oil well) are closed and (37) must be satisfied. Both problems are stated since it is usually necessary to first solve the general flow problem in order to solve the exchange flow problem.

## 3. Properties of the axial velocity solution

Although the yield stresses vary with $(y, z)$ in (36), the underlying problem is not much changed from that with constant yield stresses, which has been analysed extensively in [12–13]. The results in this section are proven straightforwardly by the same methods as in either of [12–13] for the constant yield stress problem.

THEOREM 1. *The variational inequality*

$$a(u, v-u) + j(v) - j(u) \geqslant L(v-u), \quad \forall v \in H^1_0(\Omega), \;\; u \in H^1_0(\Omega),$$

*has a unique solution.*

### 3.1. Dependence of $u$ on $f$

For $f \in [F_1, F_2]$, denote by $u_f$ the solution to (36). The following three results give a constructive method for proving the existence of a solution to the exchange flow solution. The simple methodology is to show first that the functional $Q(u_f)$ is continuous and increasing. Secondly, if there is an interval $f \in (F_1, F_2)$ with $Q(u_{F_1}) < 0$ and $Q(u_{F_2}) > 0$, there must be a solution to the general problem satisfying (37), i.e. a solution to the exchange flow problem.

LEMMA 1. *The function $f \to u_f$ is Lipschitz continuous from $f \mapsto H^1_0(\Omega)$.*

LEMMA 2. *For $f_1 < f_2$ with $f_1, f_2 \in [F_1, F_2]$, either $Q(u_{f_2}) > Q(u_{f_1})$ or $u_{f_2} = u_{f_1}$. If $u_{f_2} = u_{f_1}$, then $Q(u_{f_2}) = Q(u_{f_1}) = 0$.*

LEMMA 3. *There exists a solution to the exchange flow problem for some $f \in (F_1, F_2)$ if and only if*

$$\cos\beta Q_m(u_{F_1}) < a(u_{F_1}, u_{F_1}) + j(u_{F_1}), \tag{38}$$

$$-\cos\beta Q_c(u_{F_2}) < a(u_{F_2}, u_{F_2}) + j(u_{F_2}), \tag{39}$$

*are satisfied, or equivalently, $Q(u_{F_1}) < 0$ and $Q(u_{F_2}) > 0$.*

Having established that an exchange flow exists, the solutions have some interesting properties. Let $(f^*, u_{f^*})$ solve the exchange flow problem for $\cos\beta > 0$. First of all, and perhaps obviously, the volume flux in the (lighter) mud phase is positive and that in the cement phase is negative. Secondly, the pressure gradient $f^*$ appears to minimise the viscous dissipation functional.

PROPOSITION 1. *$Q_m(u_{f^*}) \geqslant 0$ and $Q_c(u_{f^*}) \leqslant 0$ with $Q_m(u_{f^*}) > 0$ and $Q_c(u_{f^*}) < 0$ unless $u_{f^*} = 0$.*

LEMMA 4. *The function $f = a(u_f, u_f)$ is decreasing for $f < f^*$ and is increasing for $f > f^*$. If $f^* \in (F_1, F_2)$ is the unique value for which the exchange flow constraint is satisfied, then $f = a(u_f, u_f)$ is strictly decreasing for $f < f^*$ and is strictly increasing for $f > f^*$.*

### 3.2. Dependence of $u$ on the reduced yield stresses

For fixed $f \in [F_1, F_2]$, let $(\tau_{c,R1}, \tau_{m,R1})$ and $(\tau_{c,R2}, \tau_{m,R2})$ be strictly positive, bounded continuous functions and denote by $u_{\tau_1}$ and $u_{\tau_2}$ respectively, the two solutions of (36) corresponding to the two different reduced yield stress functions. Since these functions are only defined on their respective fluid domains, define the following norm

$$\|(\tau_{c,R1}, \tau_{m,R1}) - (\tau_{c,R2}, \tau_{m,R2})\|_{L^2(\Omega)} \equiv \|\tau_{c,R1} - \tau_{c,R2}\|_{L^2_{\Omega_c}} + \|\tau_{m,R1} - \tau_{m,R2}\|_{L^2_{\Omega_m}}. \tag{40}$$

We show that the solution varies continuously with the reduced yield stresses and also that the solution (in fact the functional $a(u_\tau, u_\tau)$) decreases as the size of the reduced yield stresses increases. The imposed stresses $\tau_{k,n}(y, z)$ are bounded and the monotonicity result (see Lemma 6) indicates that for sufficiently large yield stresses there should be no flow, as is intuitive. To find the limit, an upper bound for the imposed stresses $\tau_{k,n}(y, z)$ is used. This upper bound defines minimum values for $\tau_{k,R}(y, z)$. The problem with constant (minimum) yield stresses has been analysed in [13] and bounds for there to be no flow have been established. By this methodology, we are therefore able to give an estimate for the size of yield stresses necessary to give $u = 0$.

LEMMA 5. *There exist strictly positive constants $C_1$ and $C_2$ such that*

$$a(u_{\tau_1} - u_{\tau_2}, u_{\tau_1} - u_{\tau_2}) \leqslant C_1\|(\tau_{c,R1}, \tau_{m,R1}) - (\tau_{c,R2}, \tau_{m,R2})\|^2_{L^2(\Omega)}, \tag{41}$$

$$\|u_{\tau_1} - u_{\tau_2}\|_{H^1(\Omega)} \leqslant C_2 \|(\tau_{c,R1}, \tau_{m,R1}) - (\tau_{c,R2}, \tau_{m,R2})\|_{L^2(\Omega)}. \tag{42}$$

*Proof.* Inequality (36) holds for $u = u_{\tau_1}$, $v = u_{\tau_2}$ as well as for $u = u_{\tau_2}$, $v = u_{\tau_2}$. Adding the two inequalities gives

$$\begin{aligned} a(u_{\tau_2} - u_{\tau_1}, u_{\tau_2} - u_{\tau_1}) \;\leqslant\; & \int_{\Omega_c} [\tau_{c,R1} - \tau_{c,R2}][\dot\gamma(u_{\tau_2}) - \dot\gamma(u_{\tau_1})]\,\mathrm{d}\Omega \\ & + \int_{\Omega_m} [\tau_{m,R1} - \tau_{m,R2}][\dot\gamma(u_{\tau_2}) - \dot\gamma(u_{\tau_1})]\,\mathrm{d}\Omega. \end{aligned}$$

Using the convexity of $\dot\gamma(\cdot)$ and then the Cauchy–Schwarz inequality

$$\begin{aligned} a(u_{\tau_2} - u_{\tau_1}, u_{\tau_2} - u_{\tau_1}) \;\leqslant\; & \int_{\Omega_c} |\tau_{c,R1} - \tau_{c,R2}| \dot\gamma(u_{\tau_2} - u_{\tau_1})\,\mathrm{d}\Omega \\ & + \int_{\Omega_m} |\tau_{m,R1} - \tau_{m,R2}| \dot\gamma(u_{\tau_2} - u_{\tau_1})\,\mathrm{d}\Omega \\ \leqslant\; & \|\tau_{c,R1} - \tau_{c,R2}\|_{L^2_{\Omega_c}} [a_c(u_{\tau_2} - u_{\tau_1}, u_{\tau_2} - u_{\tau_1})]^{1/2} \\ & + \|\tau_{m,R1} - \tau_{m,R2}\|_{L^2_{\Omega_m}} [a_m(u_{\tau_2} - u_{\tau_1}, u_{\tau_2} - u_{\tau_1})]^{1/2} \\ \leqslant\; & \|(\tau_{c,R1}, \tau_{m,R1}) - (\tau_{c,R2}, \tau_{m,R2})\|_{L^2(\Omega)} \\ & \times [a_0(u_{\tau_2} - u_{\tau_1}, u_{\tau_2} - u_{\tau_1})]^{1/2}. \end{aligned}$$

Thus, $C_1 = 1/\min\{\mu_k\}$. The second part of the theorem results directly from the ellipticity of $a_0(\cdot,\cdot)$, consequently also that of $a(\cdot,\cdot)$, and the continuity result for $a(\cdot,\cdot)$.

For the following result let $(\tau_{c,R}, \tau_{m,R})$ be strictly positive, continuous functions, bounded from zero by constants $(\tau_{c,R,\min}, \tau_{m,R,\min})$. Assuming $\cos\beta > 0$, suppose that the exchange flow problems corresponding to $(\tau_{c,R1}, \tau_{m,R1}) = (\tau_{c,R}, \tau_{m,R})$ and $(\tau_{c,R2}, \tau_{m,R2}) = (\tau_{c,R,\min}, \tau_{m,R,\min})$ have the solutions $(f_1^*, u_{\tau_1})$ and $(f_2^*, u_{\tau_2})$, respectively.[3]

LEMMA 6. *For exchange flow solutions* $(f_1^*, u_{\tau_1})$ *and* $(f_2^*, u_{\tau_2})$ *as described above*

$$a(u_{\tau_1}, u_{\tau_1}) \leqslant a(u_{\tau_2}, u_{\tau_2}).$$

*Proof.* First note in (36) that for any exchange flow solution $u$

$$L(u) \equiv \cos\beta\, Q_m(u),$$

and the test space for the variational problem can be reduced to $\Psi(\Omega)$

$$\Psi(\Omega) \equiv \{v \in H_0^1(\Omega) : Q(v) = 0\}.$$

In place of (36), the variational problem is as follows

$$a(u, v - u) + j(v) - j(u) \geqslant \cos\beta\, Q_m(v - u), \quad \forall v \in \Psi(\Omega), u \in \Psi(\Omega). \tag{43}$$

[3] The proof of Lemma 6 also follows through with the condition $\tau_{k,R1}(y,z) > \tau_{k,R2}(y,z)$, $\forall (y,z) \in \Omega_k$, so that $a(u_\tau, u_\tau)$ decreases with the size of (reduced) yield stresses.

A solution $u_\tau$ to (43) satisfies

$$a(u_\tau, u_\tau) + j(u_\tau) = \cos\beta Q_m(u_\tau),$$

(put $v = 0$ and $v = 2u_\tau$ into (43) and add). The problem (43) is also equivalent to minimising the functional $J_\tau(v)$

$$J_\tau(v) \equiv \tfrac{1}{2}a(v, v) + j(v) - \cos\beta\, Q_m(v), \quad v \in \Psi(\Omega), \tag{44}$$

see *e.g.* [15, Chapter 1, Sections 1.1 and 1.2] and [3, Chapter 1]. Consequently

$$-\tfrac{1}{2}a(u_{\tau_1}, u_{\tau_1}) = J_{\tau_1}(u_{\tau_1}), \qquad -\tfrac{1}{2}a(u_{\tau_2}, u_{\tau_2}) = J_{\tau_2}(u_{\tau_2}).$$

For arbitrary $v \in \Psi(\Omega)$,

$$J_{\tau_2}(v) - J_{\tau_1}(v) = \int_{\Omega_c} [\tau_{c,R2} - \tau_{c,R1}]\dot{\gamma}(v)\,\mathrm{d}\Omega + \int_{\Omega_m} [\tau_{m,R2} - \tau_{m,R1}]\dot{\gamma}(v)\,\mathrm{d}\Omega \leqslant 0.$$

Consequently

$$-\tfrac{1}{2}a(u_{\tau_1}, u_{\tau_1}) = J_{\tau_1}(u_{\tau_1}) = \inf_{v\in\Psi(\Omega)} J_{\tau_1}(v) \leqslant \inf_{v\in\Psi(\Omega)} J_{\tau_2}(v) = J_{\tau_2}(u_{\tau_2}) = -\tfrac{1}{2}a(u_{\tau_2}, u_{\tau_2}).$$

## 4. Stress minimisation principles

As well as the rate of strain minimisation principle (44), Bingham fluid flows such as those considered here will typically satisfy a stress minimisation principle. A three-dimensional version of this minimisation principle for the slow flow of a single Bingham fluid is derived in [16]. Whilst the rate of strain minimisation is equivalent to the variational formulation and yields a unique solution, the stress minimisation principle does not in general yield a unique stress field. Thus for example, Beris *et al.* [17] employ the stress minimisation principle simply as a check on the accuracy of their numerical method. The three-dimensional stress minimisation principle in [16] can be straightforwardly generalised to slow flows of two Bingham fluids that satisfy stress continuity conditions at the interface. Thus, the expression

$$\begin{aligned} K(\tilde{\boldsymbol{\tau}}) \;\equiv\; & \frac{1}{\mu_c}\int_{V_c} [|\tilde{\tau} - \tau_{c,Y}| + \tilde{\tau} - \tau_{c,Y}]^2\,\mathrm{d}V \\ & + \frac{1}{\mu_m}\int_{V_m} [|\tilde{\tau} - \tau_{m,Y}| + \tilde{\tau} - \tau_{m,Y}]^2\,\mathrm{d}V, \end{aligned} \tag{45}$$

is minimised over all admissible deviatoric stress tensors, $\tilde{\boldsymbol{\tau}}$, (*i.e.* $\tilde{\boldsymbol{\tau}}$ should satisfy the slow flow equations in each fluid domain, stress continuity conditions at the interface and have zero traction sufficiently far from the flow region, see [16]).

Whilst the above is a quite general result, a stress minimisation principle may also be derived for the shear flows considered in the previous section, which are uniaxial but not necessarily slow. For fixed $\Omega_c$ and $\Omega_m$, separated by piecewise smooth boundaries with associated normal vector $\mathbf{n} = (n_y, n_z)$, let a shear stress vector $\tilde{\boldsymbol{\tau}}(y, z)$

$$\tilde{\boldsymbol{\tau}} = (\tilde{\tau}_y, \tilde{\tau}_z),$$

be called *admissible* if it satisfies

$$\cos\beta - \tilde{f} = \frac{\partial \tilde{\tau}_y}{\partial y} + \frac{\partial \tilde{\tau}_z}{\partial z}, \quad (y,z) \in \Omega_c, \tag{46}$$

$$-\tilde{f} = \frac{\partial \tilde{\tau}_y}{\partial y} + \frac{\partial \tilde{\tau}_z}{\partial z}, \quad (y,z) \in \Omega_m, \tag{47}$$

$$[n_y\tilde{\tau}_y + n_z\tilde{\tau}_z]_c = [n_y\tilde{\tau}_y + n_z\tilde{\tau}_z]_m, \quad (y,z) \in \Gamma_i, \tag{48}$$

for a constant $\tilde{f}$. In (48) the subscripts denote the limiting values at each side of the interface $\Gamma_i$.

For an admissible shear stress vector $\tilde{\boldsymbol{\tau}}(y,z)$ and given positive yield stress function $\tilde{\tau}_R(y,z)$, (assumed continuous on each fluid domain, $\Omega_k$), define a rate of strain vector, $\tilde{\dot{\boldsymbol{\gamma}}} = (\tilde{\dot{\gamma}}_y, \tilde{\dot{\gamma}}_z)$, by

$$\tilde{\dot{\gamma}}_j = \begin{cases} \dfrac{1}{\mu_k}\left[1 - \dfrac{\tilde{\tau}_R}{\tilde{\tau}}\right]\tilde{\tau}_j, & \tilde{\tau} > \tilde{\tau}_R, \quad (y,z) \in \Omega_k, \quad k = c,m, \quad j = y,z, \\ 0, & \tilde{\tau} \leqslant \tilde{\tau}_R, \quad (y,z) \in \Omega_k, \quad k = c,m, \quad j = y,z, \end{cases} \tag{49}$$

where

$$\tilde{\tau} \equiv [\tilde{\tau}_y^2 + \tilde{\tau}_z^2]^{1/2}. \tag{50}$$

The rate of strain $\tilde{\dot{\boldsymbol{\gamma}}}$ can clearly be integrated to give an axial velocity. However, there is no guarantee that such a velocity will be continuous at the interface or satisfy the boundary conditions (22). Note that a classical solution to the exchange flow problem has the associated admissible shear stress vector $\boldsymbol{\tau}$

$$\boldsymbol{\tau} = (\tau_y, \tau_z) \equiv (\tau_{k,xy}, \tau_{k,xz}), \quad (y,z) \in \Omega_k, \quad k = c,m, \tag{51}$$

see equations (15), (16) and (21). Suppose that a solution $u$ to the exchange flow problem exists. Note that

$$0 = \int_{\Omega_c} \frac{\partial u}{\partial y}(\tau_y - \tilde{\tau}_y) + \frac{\partial u}{\partial z}(\tau_z - \tilde{\tau}_z)\,\mathrm{d}\Omega + \int_{\Omega_m} \frac{\partial u}{\partial y}(\tau_y - \tilde{\tau}_y) + \frac{\partial u}{\partial z}(\tau_z - \tilde{\tau}_z)\,\mathrm{d}\Omega. \tag{52}$$

This follows from Green's theorem in the plane, equations (46–48) and the exchange flow constraint (37). Note that the value of $\tilde{f}$ and the positive function $\tilde{\tau}_R(y,z)$ that are associated with the vector $\tilde{\boldsymbol{\tau}}(y,z)$ in (52) are completely arbitrary.

LEMMA 7. *Let $u$ be a classical solution to the exchange flow problem, with solution shear stress vector $\boldsymbol{\tau}$. Amongst all admissible shear stress vectors $\tilde{\boldsymbol{\tau}}$, the solution shear stress vector $\boldsymbol{\tau}$ minimises the expression*

$$K(\tilde{\boldsymbol{\tau}}) \equiv \frac{1}{\mu_c}\int_{\Omega_c} [|\tilde{\tau} - \tilde{\tau}_R| + \tilde{\tau} - \tilde{\tau}_R]^2\,\mathrm{d}\Omega + \frac{1}{\mu_m}\int_{\Omega_m} [|\tilde{\tau} - \tilde{\tau}_R| + \tilde{\tau} - \tilde{\tau}_R]^2\,\mathrm{d}\Omega, \tag{53}$$

*for all choices of* $\tilde{\tau}_R$ *for which*

$$\tilde{\tau}_R(y,z) \leqslant \tau_{k,R}(y,z), \quad (y,z) \in \Omega_k: \quad k = c, m. \tag{54}$$

*Proof.* Consider the expression $K(\tilde{\boldsymbol{\tau}}) - K(\boldsymbol{\tau})$ and add twice equation (52) to give

$$K(\tilde{\boldsymbol{\tau}}) - K(\boldsymbol{\tau}) = \sum_{k=c,m} \frac{1}{\mu_k} \int_{\Omega_k} I(y,z)\, \mathrm{d}\Omega,$$

where

$$I(y,z) = \tfrac{1}{4}[|\tilde{\tau} - \tilde{\tau}_R| + \tilde{\tau} - \tilde{\tau}_R]^2 - \tfrac{1}{4}[|\tau - \tau_{k,R}| + \tau - \tau_{k,R}]^2 + 2\mu_k \sum_{j=y,z} \dot{\gamma}_j(\tau_j - \tilde{\tau}_j).$$

Four cases must be considered, to show that $I(y,z) \geqslant 0$ in $\Omega$.

(1) $\tilde{\tau}(y,z) \leqslant \tilde{\tau}_R(y,z)$ and $\tau(y,z) \leqslant \tau_{k,R}(y,z)$,
(2) $\tilde{\tau}(y,z) > \tilde{\tau}_R(y,z)$ and $\tau(y,z) \leqslant \tau_{k,R}(y,z)$,
(3) $\tilde{\tau}(y,z) \leqslant \tilde{\tau}_R(y,z)$ and $\tau(y,z) > \tau_{k,R}(y,z)$,
(4) $\tilde{\tau}(y,z) > \tilde{\tau}_R(y,z)$ and $\tau(y,z) > \tau_{k,R}(y,z)$.

In case 1, $I(y,z) \equiv 0$. For case 2, $\dot{\gamma}_j = 0$ and

$$I(y,z) = \tfrac{1}{4}[|\tilde{\tau} - \tilde{\tau}_R| + \tilde{\tau} - \tilde{\tau}_R]^2 > 0.$$

For cases 3 and 4, using (49), we write $I(y,z)$ as

$$\begin{aligned} I(y,z) \;&=\; \tfrac{1}{4}[|\tilde{\tau} - \tilde{\tau}_R| + \tilde{\tau} - \tilde{\tau}_R]^2 - \tfrac{1}{4}[|\tau - \tau_{k,R}| + \tau - \tau_{k,R}]^2 \\ &\quad +2\left[1 - \frac{\tau_{k,R}}{\tau}\right] \sum_{j=y,z} \tau_j(\tau_j - \tilde{\tau}_j). \end{aligned}$$

For case 3, this becomes

$$\begin{aligned} I(y,z) \;&=\; \left[1 - \frac{\tau_{k,R}}{\tau}\right] \left[\tau^2 + \tau\tau_{k,R} - 2\sum_{j=y,z} \tau_j \tilde{\tau}_j\right] \\ &\geqslant\; \left[1 - \frac{\tau_{k,R}}{\tau}\right] \left[\tau^2 + \tau\tau_{k,R} - 2\tau\tilde{\tau}\right] \geqslant 0, \end{aligned}$$

where the Cauchy–Schwarz inequality has been used between lines 1 and 2. Finally, for case 4

$$\begin{aligned} I(y,z) \;&=\; [\tilde{\tau} - \tilde{\tau}_R]^2 - [\tau - \tau_{k,R}]^2 + 2\tau^2 - 2\tau\tau_{k,R} - 2\left[1 - \frac{\tau_{k,R}}{\tau}\right] \sum_{j=y,z} \tau_j \tilde{\tau}_j \\ &=\; \sum_{j=y,z} (\tilde{\tau}_j - \tau_j)^2 - 2\frac{\tau_{k,R}}{\tau} \left[\tilde{\tau}\tau - \sum_{j=y,z} \tau_j \tilde{\tau}_j\right] + [\tilde{\tau} - \tilde{\tau}_R]^2 - [\tilde{\tau} - \tau_{k,R}]^2 \\ &\geqslant\; \sum_{j=y,z} (\tilde{\tau}_j - \tau_j)^2 - 2\frac{\tau_{k,R}}{\tau} \left[\tilde{\tau}\tau - \sum_{j=y,z} \tau_j \tilde{\tau}_j\right] \end{aligned}$$

$$\geqslant \sum_{j=y,z} (\tilde{\tau}_j - \tau_j)^2 - 2\left[\tilde{\tau}\tau - \sum_{j=y,z} \tau_j \tilde{\tau}_j\right]$$

$$= [\tilde{\tau} - \tau]^2 \geqslant 0.$$

## 5. Conditions for $u = 0$

In accordance with the simple dimensional analysis in the introduction, the aim here is to derive a surface in the positive octant of the three-dimensional $(\beta, \tau_{c,Y}, \tau_{m,Y})$-space, which defines where $u = 0$ for the type of flows considered. The methodology used is not rigorous, but is believed to give a conservative *engineering estimate* for such a surface. This is confirmed by experiment (Section 6) and is considered quite suitable for application.

The stress minimisation principles in Section 4 effectively mean that the flow will not yield unless it has to. The axial shear flow problem that has been considered in [12–13] corresponds to the problem of Section 3 with imposed stresses $\tau_{k,n}(y, z) = 0$. This problem is perfectly well defined and, together with the three-dimensional stress minimisation principle (45), this suggests that there is no mechanism for the generation of nonzero $\tau_{k,n}(y, z)$ within $V$, for the flows considered in this paper. Thus, generation of nonzero $\tau_{k,n}(y, z)$ is associated with the transitional end regions of the volume $V$. The main characteristic of these end regions is that the interface is no longer near-parallel to the pipe axis. For an interface perpendicular to the pipe axis, continuity of normal stresses implies

$$-p_c + \tau_{c,xx} = -p_m + \tau_{m,xx}, \tag{55}$$

and the difference in static pressures on either side of the interface suggests that

$$p_c - p_m \sim \sin\beta. \tag{56}$$

Thus, where the interface is perpendicular to the pipe axis, an estimate of form

$$A_c \tau_{c,n,\max} + A_m \tau_{m,n,\max} \leqslant \sin\beta, \tag{57}$$

should be valid for the maximum stresses (where $A_c$ and $A_m$ are given constants). By considering the static deviatoric stress distribution in an inclined uniform slot, in which the two fluids are separated by a flat interface, perpendicular to the axis of the slot, it is possible to derive the estimate

$$\tfrac{1}{4}[\tau_{c,n,\max} + \tau_{m,n,\max}] \leqslant \sin\beta, \tag{58}$$

and it seems reasonable to apply this same estimate to the pipe geometry (*i.e.*, with a pipe diameter equal to the slot width), for which it will certainly be conservative.

If $\tau_{k,n} \leqslant \tau_{k,n,\max} < \tau_{k,Y}$ for each fluid, then the flow will not yield if the flow with (minimum) constant reduced yield stresses $\tau_{k,R,\min}$ defined by

$$\tau_{k,R,\min} \equiv [\tau_{k,Y}^2 - \tau_{k,n,\max}^2]^{1/2}, \tag{59}$$

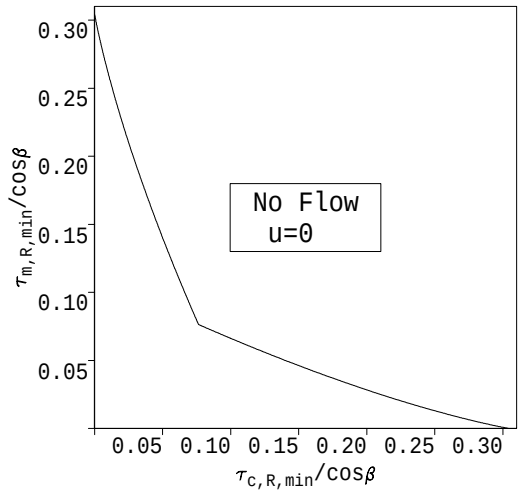


*Figure 4*. No-flow curve for constant yield stress exchange flows with simply connected $\Omega_k$ that touch the walls of the pipe.

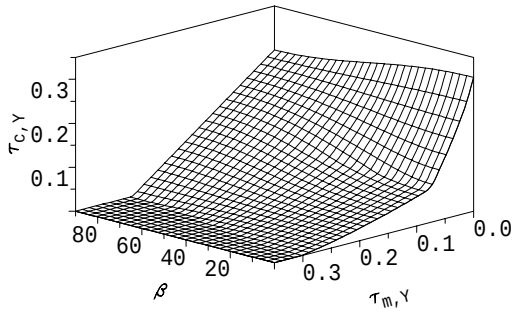


*Figure 5*. The no-flow surface $\tau_Y = \tau_{Y,0}(\theta, \beta)$, shown in the positive octant of the three-dimensional $(\beta, \tau_{c,Y}, \tau_{m,Y})$-space.

does not yield. This follows from Lemma 6 (and for a classical solution see also Lemma 7). Constant yield stress stratified axial exchange flows in a pipe are considered in [12–13]. Considering all simply connected $\Omega_k$ that touch the walls of the pipe, the constant yield stress axial exchange flow will not yield if the magnitude of the vector $(\tau_{c,R,\min}/\cos\beta,\ \tau_{m,R,\min}/\cos\beta)$ exceeds the curve shown in Figure 4, see [13] for a derivation.

This result is not justified rigorously for completely general $\Omega_k$, since there exists the possibility of a very large yield stress fluid (*e.g.*, a solid), moving down the centre of the pipe whilst never touching the walls. In reality such a situation is not observed to evolve from initial conditions such as those in Figure 1. Firstly, the larger yield stress fluid appears to be difficult to displace from the walls. Secondly, even if such a flow is initiated, gravity tends to force the heavier fluid into contact with the lower walls and the lighter fluids into contact with the upper wall.

Define a polar coordinate system $(\tau_Y, \theta)$ in the positive quadrant of the yield stress plane, by

$$\tau_Y \equiv [\tau_{c,Y}^2 + \tau_{m,Y}^2]^{1/2}, \qquad \tan\left(\frac{\pi}{4} - \theta\right) \equiv \frac{\tau_{m,Y}}{\tau_{c,Y}}. \tag{60}$$

The curve (58) and that in Figure 4 can be written as

$$[\tau_{c,n,\max}^2 + \tau_{m,n,\max}^2]^{1/2} = \tau_{n,Y}(\theta)\sin\beta, \tag{61}$$

$$[\tau_{c,R,\min}^2 + \tau_{m,R,\min}^2]^{1/2} = \tau_{s,Y}(\theta)\cos\beta \tag{62}$$

there is no simple analytical expression for $\tau_{s,Y}(\theta)$, see [13]. When it is assumed that, if the maximum normal deviatoric stress terms lie on (61), to ensure that $u = 0$, it will be sufficient for the minimum reduced yield stresses to lie on the curve (62), the estimates for the diagonal and nondiagonal deviatoric stresses can be combined to give the surface in Figure 5. This surface is defined simply by

$$\tau_Y = \tau_{Y,0}(\theta, \beta) \equiv ([\tau_{n,Y}(\theta)\sin\beta]^2 + [\tau_{s,Y}(\theta)\cos\beta]^2)^{1/2}. \tag{63}$$

For values of $(\tau_{c,Y}, \tau_{m,Y})$ which lie above the curve $\tau_Y = \tau_{Y,0}(\theta, \beta)$, it is expected that a flow will not be initiated.

## 6. Experimental comparison

A series of static stability experiments were performed to compare with the surface (63). The basic experiment performed consists of a long closed-ended pipe half-filled with each of two fluids, separated by an interface which is perpendicular to the pipe axis. The heavier fluid was positioned above the lighter fluid and motion of the fluid-fluid interface was observed. Any movement of the fluid-fluid interface was regarded as evidence of instability. A range of pipe diameters, pipe inclinations, densities and rheologies were tested. A single experiment consists of testing one set of rheological parameters for a fixed geometry, pipe inclination and fluid densities. Experiments with a given geometry and density difference were repeated with progressively larger yield stress fluids until the interfaces were found to be stable. Each sequence of experiments thus leads to a single experimental point which lies on the marginal stability surface for an interface that is perpendicular to the pipe axis.

Two types of fluid were used. When a fluid without a yield stress was required, a Xanthan gum solution was used. At very low shear rates, less than $10^{-3}\,\mathrm{s}^{-1}$, this is approximately Newtonian but it becomes shear thinning at higher shear rates. For fluids with a yield stress, RDS grade Laponite suspension was used. Laponite is an synthetic clay mineral related to natural clays such as hectorite or bentonite which have a similar disc shaped structure but are an order of magnitude larger, (the general formula for Laponite is $Na_{0.7}[(Mg_{5.5}Li_{0.3}Si_8)O_{20}(OH)_4]^{0.7}$). One advantage of using Laponite suspensions as an experimental fluid is their transparency. A second advantage is that Laponite has a yield stress which is to a large extent controllable by varying either the time which the suspension is allowed to gel in a static condition, or the concentration of Laponite in the suspension, or by addition of salts, ($CaCl_2$). The suspensions were also weighted with Barite to control the fluid density. All experiments were conducted using a 6 wt percent suspension of Laponite which was allowed to fully hydrate before the addition of the required concentration of $CaCl_2$.

For small diameter pipes (50·8 mm and 101·6 mm) the pipes were half-filled with the heavier fluid when vertical. The lighter fluid was then placed on top, taking care not to disturb the interface. The upper end cap of the pipe was conical, ensuring complete filling of the pipe. The tube was kept static in the stable vertical position until it was estimated that the required yield stress had developed. It was then inverted to the required inclination and left resting against an inclined board for observation of the interface position. Measurements of the yield stresses with a vane rheometer were made simultaneously on samples taken from the two fluids at the moment of inversion. In this way, a good estimate was made of the fluid yield stresses on both sides of the interface at the time when the interface stability was observed. For large diameter pipes (203·2 mm), quick inversion through more than 90 degrees was not possible. The vertical position was found to be more stable than an inclined position for the particular interface configuration used. Therefore, while keeping the pipe vertical, the heavier fluid was injected slowly on top of the lighter (yield stress) fluid, using a tool which diverted the flow to the sides of the pipe. After the estimated waiting time, the tube was inclined as required. This procedure seemed to work fairly well, in that when the interface failed at the larger deviations, fluid motion was rapid, but the yield stresses developed before injection of

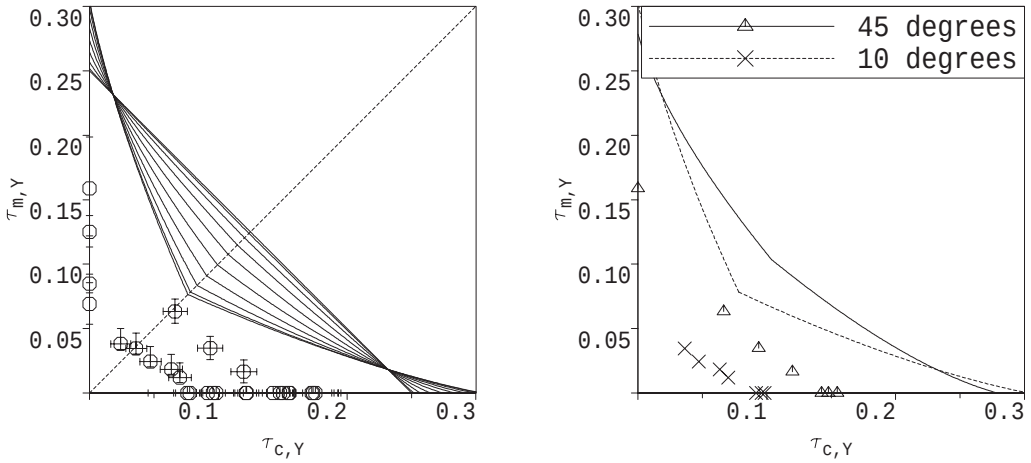


(a) (b)

*Figure 6.* Comparison of experimental results with the no-flow surface $\tau_Y = \tau_{Y,0}(\theta, \beta)$: (a) results with maximum error estimates and sections through the surface (63) at 10 degree intervals; (b) results for $\beta = 10$ degrees and $\beta = 45$ degrees.

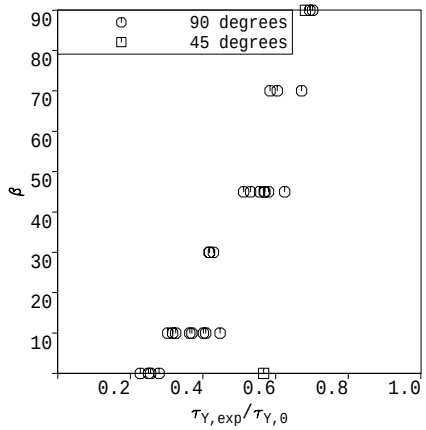


*Figure 7.* Variation of $\tau_{Y,\text{exp}}/\tau_{Y,0}(\theta, \beta)$ with inclination $\beta$ for all experimental data with interface inclined at 90 degrees to the pipe axis. Also shown are the results of two sequences of experiments with interface inclined at 45 degrees to the pipe axis.

the denser fluid were sufficient to prevent motion for the (mechanically unstable) horizontal interface in the vertical pipe.

### 6.1. RESULTS

A number of sequences of experiments were conducted, each giving rise to values $(\tau_{c,Y}, \tau_{m,Y})$, lying on the (experimental) marginal stability surface for the perpendicular fluid-fluid interface. It was also possible to make some estimate of the maximum measurement error in $(\tau_{c,Y}, \tau_{m,Y})$. Figure 6(a) shows the experimental yield stresses on the marginal stability surface, together with error bars. The lines drawn in Figure 6(a) are sections through the surface (63) at 10 degree intervals. For more detail, Figure 6(b) shows the same comparison, but made with only the data at 10 degree and 45 degree pipe inclinations from vertical. It is re-emphasised that each point plotted in Figure 6 corresponds to whole a sequence of experiments.

For all results in Figure 6 the theoretical prediction is conservative in comparison with experimental results. To study the degree of conservatism, Figure 7 plots the ratio of $\tau_{Y,\mathrm{exp}}/\tau_{Y,0}(\theta, \beta)$ for each of the experimental points, ($\tau_{Y,\mathrm{exp}}$ being the modulus of the experimentally measured yield stresses). The experimental modulus varies between about 20 and 70 percent of the theoretical value as the pipe inclination varies from vertical to horizontal. Also shown in Figure 7 are the results of two sequences of experiments with interface inclined at 45 degrees to the pipe axis. One sequence of experiments was conducted in a horizontal pipe, the other in a vertical pipe.

## 7. Discussion

The results shown in Figures 6 and 7 indicate clearly that characterisation of the (mechanically unstable) static state, for a fixed interface configuration, in terms of a marginal stability surface in the $(\beta, \tau_{c,Y}, \tau_{m,Y})$-space is both experimentally feasible and also sensible, confirming the simple dimensional analysis. The theoretical surface $\tau_Y = \tau_{Y,0}(\theta, \beta)$, in all cases gives a conservative prediction of the yield stresses required to keep the perpendicular interface static. This is to be expected and the experimental comparison should therefore be regarded as a partial validation of (63). There are a number of issues related to the conservatism of (63).

The approach taken in Section 5 has been to take a conservative estimate of the normal deviatoric stresses and combine this with a conservative estimate of the shear stresses generated in the axial shear flow. The method of combining these estimates is somewhat heuristic, but must be expected to yield a conservative prediction of conditions for $u = 0$ (*e.g.* along any interface the maximum shear and normal stresses are unlikely to be generated in exactly the same place, the individual estimates themselves will be conservative for many interfaces, *etc*). Experimental comparison serves the purpose of indicating how conservative this prediction will be for a given interface configuration. As discussed in Section 1, the problem considered will be characterised by nonuniqueness of stable static interface configurations. For the industrial application, fluid-fluid interface configuration is not controlled during a typical cement plug placement operation. These two factors have motivated the theoretical approach, *i.e.*, for practical usage it is necessary to derive estimates are valid for a practically relevant (and wide) class of possible interface configurations. This situation must be contrasted with the experimental situation, where any experiment tests only one particular initial interface configuration. For reasons of economy, it is not possible to test *all* interface configurations for any large class of surfaces. Thus, comparison of the experimental results with (63) in terms of a direct validation is not justified. Direct validation appears difficult. In [12–13] exact mathematical solutions are derived for test example flows with constant yield stresses, zero normal deviatoric stresses and geometrically simple interfaces. To engineer such flows in a laboratory with non-Newtonian fluids and realistic (*controllable*) rheologies is extremely difficult. In contrast, the flows in Section 6 are relatively easy to engineer in the laboratory, but the mathematical theory (and hence comparison) is less exact.

The experimental scatter in Figure 7 is not severe and some sort of *curve* could be fitted (if this were a sensible exercise). This and Figure 6(b) suggest that the experimental values do represent a marginal stability surface in $(\beta, \tau_{c,Y}, \tau_{m,Y})$-space. It is supposed that if a similar set of experiments was carried out for a different interface configuration, one would derive a *curve* similar to the data in Figure 7, with similar scatter. Repeating this for a range of different

interface configurations should (exhaustively) lead to a surface which is valid for an acceptably wide range of initial interfaces. This type of exhaustive search is however impractical.

To explore the effect of interface inclination a little, the two series of experiments with the interface at 45 degrees to the pipe axis were performed. These points are also plotted in Figure 7, where they can be compared with the previous 90 degree interface inclination results. For the horizontal pipe there is little effect, but for the vertical pipe the interface yields much more readily, see Figure 7. Intuitively (and perhaps simplistically), it is thought that the interface inclination which will be most unstable at different pipe inclinations, is that which is parallel to the direction of gravity, whereas that which will be most stable lies perpendicular to the direction of gravity. If this is true, then the perpendicular interface configuration tested in the majority of experiments is the worst case when the pipe is horizontal and the best case when the pipe is vertical, partly accounting for the variation in conservatism in Figure 7. Considering a practically wide range of interface inclinations that might be realised, one could infer that a surface in $(\beta, \tau_{c,Y}, \tau_{m,Y})$-space at about 70 percent of the values $\tau_Y = \tau_{Y,0}(\theta, \beta)$, would be a good estimate of the marginal stability curve. However, (63) remains a quite reasonable conservative engineering estimate of the yield stresses required to maintain an arbitrary interface statically stable between two Bingham fluids in a closed pipe.

Although there is a high confidence level in the validity of (63), this is a purely mechanical estimate of sufficient $(\tau_{c,Y}, \tau_{m,Y})$ to ensure that $u = 0$. Nothing is said about the type of interface and/or flow which is most likely to be observed when the initial interface is unstable. As evidenced in Figure 7, different interface configurations can have vastly different stability characteristics. This means that an initial interface may be unstable, but the fluids flow in such a way that the resulting interface configuration is stable and the flow stops. This was observed in some of the experiments. When the unstable flow continues, the interfaces generally tend to elongate. Flows in the end regions remain three-dimensional and can be very interesting, *e.g.* front steepening and the breaking off of regions of fluid from the main flow can be observed. A phenomena which is not modelled in this paper, nor in the previous work [11–13], is displacement at the pipe wall as the flow propagates. Generally, the fluid with the higher effective viscosity is harder to displace from the wall, so that sometimes wall layers were created (*i.e.*, the flow still becomes near uniaxial but the cross-sectional interface is multi-layered). When the pipe is vertical, there is a tendency for the interface to yield in the centre of the pipe. However, when the pipe is inclined (even slightly) the interface yields asymmetrically.

In applying the model and laboratory results to an oilfield situation, we encounter a number of additional complexities. First of all, even though the Bingham fluid model is an extremely common industry characterisation, the rheologies of cement slurries, drilling muds and other wellbore fluids are not always described accurately by the model. For this process problem, most relevant is that many of these fluids have a time and/or shear history dependant yield stress, in oilfield terms they develop a *gel strength* over time. This is not the same as yield stress, since the gel can be *broken* by initiating flow. However, the gel strength will act in the same way as the yield stress in preventing flow, *i.e.*, the gel strength must be exceeded by the deviatoric stress in order for flow to be initiated. There are many problems with predicting the gel strength of wellbore fluids thousands of metres below surface, where temperature, pressure, fluid conditioning, solids content and fluid loss can all have significant effects.

A second constraint in applying these results comes from the various mixing phenomena that are possible and which are poorly understood at present. The theory developed here depends upon long-thin and/or slow flow assumptions, *e.g.*, gentle placement of the cement slurry, probably with a flow diverter. Frequently, the flow is neither diverted nor slow during

placement. There then exists the possibility of mixing downhole, which might effectively reduce the buoyancy gradient, allowing mechanical stability at much smaller values of $\hat{\tau}_{k,Y}$. Similarly, chemical incompatibility between cement slurries and drilling muds is not uncommon. This can have the effect of *viscosifying* a thin region close to the interface. Indeed there are a range of complex phenomena which remain to be studied.

Perhaps the simplest sure way to apply the results here is in designing a fluid which develops a very large yield stress (or gel strength), very soon after placement. In many situations, a *viscous pill* fluid will be placed underneath the cement slurry, of a density which lies between the density of the drilling mud (below) and the cement slurry (above). This results in two mechanically unstable interfaces. The density and rheology of the viscous pill fluid can be designed to keep both interfaces stable, by applying (63) to each interface.

## Acknowledgements

The management of Schlumberger are thanked for their permission to publish this paper.

## References

1. R. Byron-Bird, G. C. Dai and B. J. Yarusso, The rheology and flow of viscoplastic materials. *Reviews in Chemical Engineering* 1(1) (1983) 1–70.
2. V. N. Constantinescu, *Laminar Viscous Flow.* Berlin: Springer-Verlag, Mechanical Engineering Series (1995).
3. R. Glowinski, *Numerical Methods for Nonlinear Variational Problems.* Berlin: Springer-Verlag (1983) 493 pp.
4. P. P. Mossolov and V. P. Miasnikov, Variational methods in the theory of the fluidity of a viscous plastic medium. *J. Mech. Appl. Math.* 29 (1965) 468–492.
5. R. M. Beirute. Flow behavior of an unset cement plug in place. *Society of Petroleum Engineers*, paper number, SPE 7589 (1978).
6. D. L. Bour, D. L. Sutton and P. G. Creel, Development of effective methods for placing competent cement plugs. *Society of Petroleum Engineers*, paper number, SPE 15008 (1986).
7. D. G. Calvert, J. F. Heathman and J. E. Griffith, Plug cementing: Horizontal to vertical conditions. *Society of Petroleum Engineers*, paper number, SPE 30514 (1995).
8. K. Harestad, T. P. Herigstad, A. Torsvoll, N. E. Nødland and A. Saasen, Optimization of balanced-plug cementing. *Society of Petroleum Engineers*, paper number, SPE 33084 (1997).
9. C. Marca, Remedial cementing. In: E. B. Nelson (ed.), *Well Cementing*. Schlumberger Educational Services, Houston (1990).
10. R. C. Smith, R. M. Beirute and G. B. Holman, Improved method of setting successful whipstock cement plugs. *Society of Petroleum Engineers*, paper number, SPE 11415 (1983).
11. I. A. Frigaard, Stratified exchange flows of two Bingham fluids in an inclined slot. *J. Non-Newtonian Fluid Mech.* 78 (1998) 61–87.
12. I. A. Frigaard and O. Scherzer, Uniaxial exchange flows of two Bingham fluids in a cylindrical duct. To appear in *IMA J. Appl. Math.*; accepted January 1998.
13. I. A. Frigaard and O. Scherzer, The effects of yield stress variation on uniaxial exchange flows of two Bingham fluids in a pipe. Submitted to *SIAM J. Appl. Math.*, March 1998; Technical report 6/1998, Industrial Mathematics Institute, University of Linz, Austria (1998).
14. I. C. Walton and S. H. Bittleston, The axial flow of a Bingham plastic in a narrow eccentric annulus. *J. Fluid Mech.* 222 (1991) 39–60.
15. R. Glowinski, J. L. Lions and R. Tremolieres, *Numerical Analysis of Variational Inequalities.* Amsterdam: North-Holland (1981) 776 pp.
16. W. Prager, On slow visco-plastic flow. In: *Studies in Mathematics and Mechanics.* Volume presented to Richard von Mises, Academic Press (1954) pp. 208–216.
17. A. N. Beris, J. A. Tsamopoulos, R. C. Armstrong and R. A. Brown, Creeping motion of a sphere through a Bingham plastic. *J. Fluid Mech.* 158 (1985) 219–244.